Technical Note

Ground Moving Target Detection and Estimation for Airborne Multichannel Radar Based on Coherent Difference Processing

Chong Song [1,2], Bingnan Wang [1,*], Maosheng Xiang [1], Weidi Xu [1,2], Zhongbin Wang [1,2], Yachao Wang [1] and Xiaofan Sun [3]

1   National Key Laboratory of Microwave Imaging Technology, Aerospace Information Research Institute, Chinese Academy of Sciences, Beijing 100190, China; songchong18@mails.ucas.edu.cn (C.S.); xms@mail.ie.ac.cn (M.X.); xuweidi17@mails.ucas.ac.cn (W.X.); wangzhonbin17@mails.ucas.ac.cn (Z.W.); wangyc@aircas.ac.cn (Y.W.)
2   School of Electronic, Electrical and Communication Engineering, University of Chinese Academy of Sciences, Beijing 100049, China
3   Beijing Institute of Spacecraft System Engineering, China Academy of Space Technology, Beijing 100094, China; sunxiaofan15@mails.ucas.ac.cn
*   Correspondence: wbn@mail.ie.ac.cn

Abstract: Ground moving targets with slow velocity and low radar cross-section (RCS) are usually embedded in the clutter Doppler spectrum. To achieve the detection and estimation of such targets, a novel method operating in the range-Doppler domain is developed for airborne multichannel radar systems. The interferometric phases that are sensitive to moving targets are obtained by coherent difference processing (CDP) for target detection. Moreover, the amplitude is utilized as complementary information to improve the detection performance. Then, a matched filter bank is designed and applied to the CDP processed data to complete the parameter estimation. The proposed method provides the benefits of high efficiency and robustness, since it does not involve matrix inversion, and it does not require homogeneous clutter assumption unlike adaptive algorithms. Experiments on real data acquired by an airborne X-band four-channel radar system demonstrate its effectiveness.

Keywords: coherent difference processing (CDP); matched filter bank; ground moving target indication (GMTI); airborne multichannel radar

1. Introduction

Airborne radar ground moving target indication (GMTI) has received a great deal of attention as a powerful tool to accomplish many tasks, such as activity monitoring and civil traffic management [1–3]. However, since airborne radar systems operate in a down-looking mode, the strong backscattering generated from ground clutter scatterers is superimposed, and the signal-to-clutter plus noise ratio (SCNR) may be extremely low for targets with low radar cross-section (RCS). Moreover, the Doppler spectrum of the clutter may be severely spread due to the fast motion of the platform, and slow-moving targets may be totally submerged among different Doppler channels [4]. Fortunately, compared with the inherent limitations of traditional single-channel systems, radar systems equipped with multiple channels along the track direction have more degrees of freedom (DOFs) to suppress clutter and jamming, and they are more convenient to characterize the correlated properties between data in different channels. Therefore, the applications of the multichannel airborne radar GMTI are a future development trend [5].

For fast-moving targets in the exo-clutter region, conventional methods (e.g., frequency domain filtering [6]) can be used to achieve target detection, but detecting slow-moving targets that fall in the endo-clutter region is a challenging task. Therefore, this article focuses on the detection and estimation of slow and low-RCS moving targets. In the image domain,

along-track interferometry (ATI) [1] and displaced phase center array (DPCA) [7] utilize the phase difference and amplitude for detection, respectively. For a lower signal-to-clutter ratio (SCR), the performance of the ATI detector rapidly degrades, and the performance of the DPCA detector deteriorates as the signal-to-noise ratio (SNR) decreases. Therefore, in [2], multichannel DPCA and multichannel ATI were proposed to improve the detection performance. In [8], a new multistage detector with the aim of addressing extremely heterogeneous environments was proposed on the basis of the degree of radial-velocity consistency (DRVC) test. In [9], a novel two-step scheme based on the greatest of (GO)-DPCA and local space-time adaptive processing (STAP) was proposed. However, for these methods, additional processing is necessary to generate the synthetic aperture radar (SAR) images, which is very time-consuming. Instead, using range-compressed data is very attractive because it does not involve conventional time-consuming SAR imaging. Perhaps the best-known algorithm using such data is the STAP, which suppresses clutter by adaptively combining spatial and temporal data from a short coherent processing interval (CPI) [10]; thus, full STAP is not typically used in practice. As a reduced rank algorithm of the full STAP [3], unfortunately, post-Doppler STAP (PD-STAP) also has requirements on the training data size and content (i.e., independent, identically distributed (I.I.D.) and Reed-Mullet-Brennan (RMB) rule). In [11], a standardized version of PD-STAP with a constant false alarm rate (CFAR) property, called adaptive matched filter (AMF), was presented. However, these STAP detectors are limited by training data and computational complexity. In addition, due to the assumption of homogeneous environments, heterogeneous clutter can cause deleterious effects. To address this issue, Silva compared four training data selection algorithms for clutter covariance matrix (CCM) estimation and proposed a module for moving target signal rejection, but this operation increased additional computational cost [12]. In [13], Yadin developed a GMTI scheme for two interferometric channels in the range-Doppler domain, where clutter suppression can be applied to the detection but not to the relocation process.

To address the aforementioned issues, a novel algorithm operating in the range-Doppler domain was developed for airborne multichannel radar systems. On the basis of the proposed coherent difference processing (CDP), interferometric phases that are sensitive to moving targets are obtained to achieve the detection and estimation of targets, and the amplitude information is used in a complementary manner to reduce the false alarm rate. Since the interferometric phase is usually heavily compromised by strong ground clutter, we adopted multichannel DPCA to suppress the clutter before the CDP. It is demonstrated here that the proposed method has high detection performance and environmental robustness in practical applications.

This paper is arranged as follows: the multichannel signal model is developed in Section 2. In Section 3, the theory of the proposed method and its mathematical framework are introduced. Moreover, the computation complexity is analyzed. The experimental results are presented in Section 4. Section 5 concludes this study.

2. Multichannel Signal Model

Assume that the side-looking multichannel radar system has n spatial channels in azimuth; the first channel serves as a reference channel, as shown in Figure 1. The radar platform flies at a fixed altitude H, and the target is assumed to move with constant velocities V_x and V_y along the X- and Y-axes, respectively. $R(t)$ is the range between the first channel and the target as a function of slow time t. Under the far-field hypothesis, the received and range-compressed signal by the n-th channel can be modeled as

$$s_n(t) = \alpha_s w_n(t) e^{-2j\beta R(t)} e^{-j\beta u(t)b_n}, \tag{1}$$

where α_s is the complex amplitude of the target, $\beta = 2\pi/\lambda$ is the wavenumber, λ is the radar wavelength, $w_n(t)$ is the two-way antenna pattern of the n-th channel, $b_n(b_1 = 0)$ is the n-th physical baseline length, $u(t) = \cos(\theta)$ is the directional cosine, and θ is the

direction-of-arrival (DOA) angle since the squint angle is assumed to be zero, as shown in Figure 1.
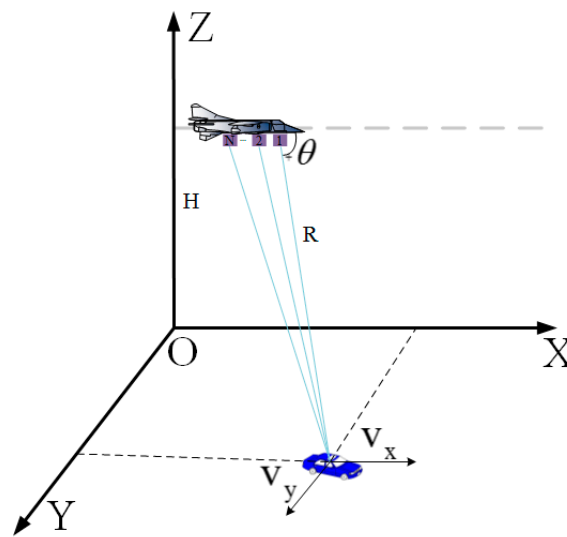

Figure 1. Geometry of the multichannel radar system.

Using the fast Fourier transform (FFT), the signal model in Equation (1) can be transformed into the range-Doppler domain as follows:

$$S_n(f_a) = \alpha_s W_n(f_a) e^{-2j\beta R(f_a)} e^{-j\beta u(f_a) b_n}, \tag{2}$$

where f_a is the Doppler frequency bin. $W_n(f_a)$ is the Doppler-domain expression of the $w_n(t)$, and they own the same shape.

Since the directional cosine of the target is related to its Doppler frequency and line-of-sight velocity, it can be expressed as follows:

$$u(f_a) = \cos(\theta) = \frac{\lambda f_a}{2v_p} + \frac{v_r}{v_p}, \tag{3}$$

where v_p is the platform velocity, and v_r is the radial velocity of the moving target. If the radial velocity is estimated, the DOA angle can be calculated using Equation (3).

According to Equations (2) and (3), after compensating for the interferometric phases among different Doppler cells, the signal can be expressed as follows:

$$S_n(f_a) = \alpha_s W_n(f_a) e^{-2j\beta R(f_a)} e^{-j\pi \frac{2v_r b_n}{\lambda v_p}}. \tag{4}$$

The phase differences among channels are mainly related to v_r, which is different from stationary clutter.

3. Proposed Method for Target Detection and Estimation

In the range-Doppler domain, the moving target should remain in one Doppler bin during the CPI to optimize the computational cost, which results in the number of pulses $N_a = \frac{PRF\sqrt{\lambda R}}{\sqrt{2}v_P}$ (PRF is the pulse repetition frequency) [3]. The proposed framework is shown in Figure 2. In practical applications, data preprocessing is necessary to improve the detection performance. The preprocessing contains platform motion compensation [14], range compression, range-cell migration correction [15], antenna pattern calibration, and phase compensation [16]. Traditional methods are utilized for data preprocessing since they are not the main research content.
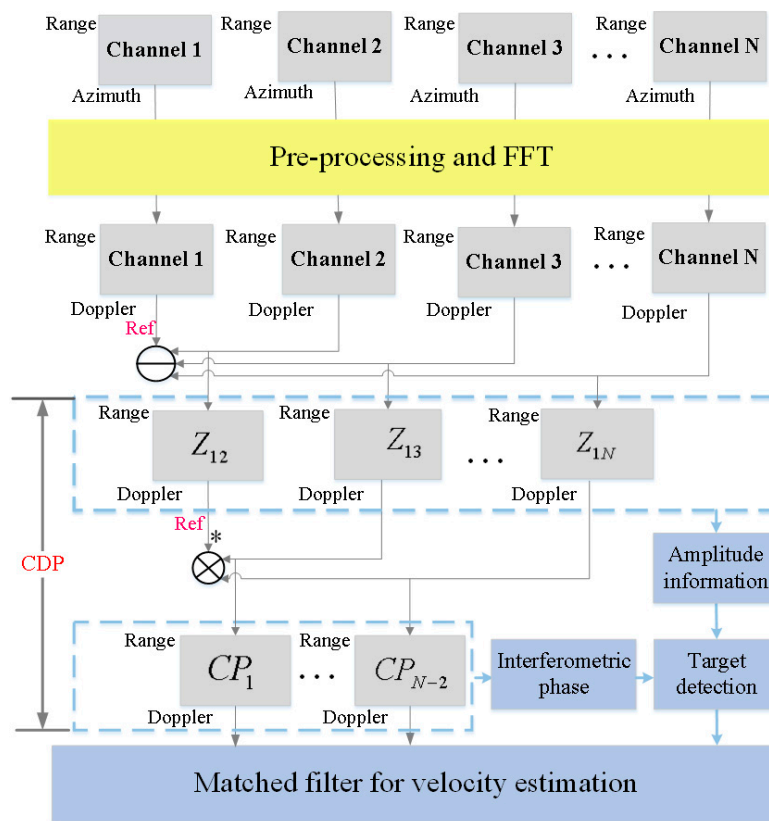
Figure 2. Framework of the proposed method.

3.1. Proposed Method

Considering the specific phase relationship required for further processing, we modify the multichannel DPCA to suppress clutter in advance. Assuming that channels are well calibrated (i.e., $W(f_a) = W_n(f_a)$), the signal of the subtraction operation between the nth channel and the first channel can be expressed as

$$
\begin{aligned}
Z_{n1}(f_a) &= S_n(f_a) - S_1(f_a) \\
&= -2\alpha_s W(f_a) e^{-2j\beta R(f_a)} \sin\left(\frac{v_r b_n}{\lambda v_p}\pi\right) e^{-j\left(\frac{v_r b_n}{\lambda v_p}\pi + \frac{\pi}{2}\right)} \quad (n > 1)
\end{aligned}
\tag{5}
$$

For stationary targets (i.e., clutter), signatures are suppressed. The energy from moving targets is not suppressed and, thus, can be detected in target pre-detection. The first detection is based on amplitude information, as shown in Equation (6).

$$
M_1(f_a) = \left[A(f_a) \underset{1}{\overset{0}{\lessgtr}} Th_A \right],
\tag{6}
$$

where Th_A is the threshold for amplitude, and $A(f_a)$ is the value generated by noncoherently adding the energy of $Z_{n1}(f_a)$. In general, the threshold can be determined by a CFAR method (i.e., adopting compound-Gaussian distribution in [17]). However, the false alarm rate is higher when purely using amplitude detection, especially when there are many strong discrete scatterers. Therefore, adopting CDP, this article utilizes the interferometric phases to achieve the second detection and takes amplitude detection as a complementary detector.

Taking the output $Z_{21}(f_a)$ in Equation (5) as the reference, the CDP is expressed as

$$CP_{n-2}(f_a) = Z_{n1}(f_a) * \text{conj}(Z_{21}(f_a))$$

$$= 4\alpha_0^2 W^2(f_a) \sin\left(\frac{v_r b_n}{\lambda v_p}\pi\right) \sin\left(\frac{v_r b_2}{\lambda v_p}\pi\right) e^{-j\pi\frac{v_r(b_{n-1}-b_2)}{\lambda v_p}} \quad (n > 2) \tag{7}$$

The phase of $CP_{n-2}(f_a)$ can be written as follows:

$$\phi_{n-2}(f_a) = \text{angle}(CP_{n-2}(f_a)) = -\frac{v_r(b_{n-1}-b_2)}{\lambda v_p}\pi \quad (n > 2). \tag{8}$$

For stationary clutter, the interferometric phase is ideally 0 after the CDP according to Equation (8). In the cell of interest, since the clutter is suppressed in advance, the interferometric phase generated by the moving target is the main component; thus, this phase information can be used to detect the moving target. When $M_1(f_a) = 1$, the second step detection is given by

$$M_2(f_a) = \sum_{n=3}^{N} \left[\phi_{n-2}(f_a) \underset{1}{\overset{0}{\lessgtr}} Th_{\phi,n-2}\right], \tag{9}$$

where $Th_{\phi,n-2}$ is the phase threshold that corresponds to $\phi_{n-2}(f_a)$. Generally, the thresholds can be decided by the CFAR method (i.e., adopting the phase statistics in [8]). If the value $M_2(f_a)$ is greater than $(N-2)/2$, which can also be determined by the actual situation, we declare target detection. The basic idea of the proposed detection scheme is to initially set a moderate threshold in Equation (6) for the amplitude detector to ensure that most true targets are detected while accepting an excessive number of false alarms. Subsequently, the phase threshold in Equation (9) is employed to remove as many of these false detections from the strong residual clutter as possible, and it ideally does not reduce the detection probability. Thus, the detection performance can be significantly improved by applying two tests, each with a moderate threshold. In addition, multiple CPIs or road information can be utilized to suppress radial scatterers if the CDP process fails [18].

After the moving targets are detected, the velocities need to be estimated to enhance the practicality. Equation (7) is rewritten in the form of a matrix as follows:

$$I_{CP} = \begin{bmatrix} CP_1(f_a) \\ CP_2(f_a) \\ \vdots \\ CP_{N-2}(f_a) \end{bmatrix} = 4\alpha_0^2 W^2(f_a) \sin\left(\frac{v_r b_2}{\lambda v_p}\pi\right) \begin{bmatrix} \sin\left(\frac{v_r b_3}{\lambda v_p}\pi\right)e^{-j\pi\frac{v_r(b_3-b_2)}{\lambda v}} \\ \sin\left(\frac{v_r b_4}{\lambda v_p}\pi\right)e^{-j\pi\frac{v_r(b_4-b_2)}{\lambda v}} \\ \vdots \\ \sin\left(\frac{v_r b_N}{\lambda v_p}\pi\right)e^{-j\pi\frac{v_r(b_N-b_2)}{\lambda v}} \end{bmatrix} \tag{10}$$

It is observed from Equation (10) that the amplitude and phase difference after the CDP are mainly related to unknown v_r for a fixed moving target. Assuming that, in the general case, no a priori information regarding the target motion is available, we design an algorithm incorporating a matched filter bank to estimate the radial velocity. The algorithm considers the possible radial velocities of the target, which synthesizes several matched filters. The possible values are limited by an interval $(-v_{r,\max}, v_{r,\max})$, where $v_{r,\max}$ is the maximum ambiguous radial velocity. The frequency resolution δf_a is inversely proportional to the time observation interval T (i.e., $T = N_a/PRF$). Thus, the 3 dB resolution is $\delta f_a = 0.88/T$, and the corresponding velocity resolution is $\delta v_r = 0.44\lambda/T$ [19,20]. The number of filters is calculated by $2v_{r,\max}/\delta v_r$.

Assuming that the target radial velocity v_l corresponds to the *l*-th matched filter, the matched filter generated according to Equation (10) is defined as follows:

$$s_l = \left[\frac{e^{-j\frac{v_l(b_3 - b_2)}{\lambda v_p}\pi}}{\sin\left(\frac{v_l b_3}{\lambda v_p}\pi\right)} \quad \frac{e^{-j\frac{v_l(b_4 - b_2)}{\lambda v_p}\pi}}{\sin\left(\frac{v_l b_4}{\lambda v_p}\pi\right)} \quad \cdots \quad \frac{e^{-j\frac{v_l(b_N - b)}{\lambda v_p}\pi}}{\sin\left(\frac{v_l b_N}{\lambda v_p}\pi\right)} \right]^T, \tag{11}$$

where $[\cdot]^T$ denotes the matrix transpose.

For the *l*-th matched filter, the target parameter estimation response is defined as follows:

$$P_{\text{out}} = |I_{CP} * \text{conj}(s_l)|_2. \tag{12}$$

Using the output response in Equation (12), the estimated target radial velocity is

$$\hat{v}_r = \underset{v_l}{\text{argmax}}(P_{\text{out}}). \tag{13}$$

Then, the corresponding DOA angle is calculated using Equation (3). According to the aforementioned steps, target detection and estimation can be completed.

3.2. Computational Complexity

In real-time applications, the computational burden is particularly important. Compared with PD-STAP, the proposed method does not have requirements for the training data. Moreover, it is computationally simpler, since PD-STAP requires the estimation and inversion of CCM. Specifically, the proposed method has a complexity of $O(N_a N_r (2N - 3) + L N_v (N - 2))$, while PD-STAP has a complexity of $O(N_a N_r (N_v (2N^2 + 2N) + KN^2 + N^3))$ [21]. N_a, N_r, N_v, $L(L \leq N_a N_r)$ andK denote the azimuth cells, range cells, dimensionality of the search parameter space, target number, and training data size, respectively. The complexity $O(N_a N_r (2N - 3))$ of the proposed method is due to the multichannel DPCA and CDP, and the complexity$O(L N_v (N - 2))$ represents the matched filters for the parameter estimation of the detected moving targets. The complexity$O(N_a N_r (KN^2 + N^3))$ of PD-STAP is due to the CCM estimation and inversion, and the $O(N_a N_r N_v (2N^2 + 2N))$ complexity is due to statistical calculations.

4. Experimental Results

To demonstrate the validation of the proposed method, we present simulations and experimental results using airborne X-band four-channel radar data.

4.1. Performance Analysis

The multichannel radar system parameters (see Table 1) were adopted to analyze the performance of the proposed method using the receiver operating characteristic curve (ROC curve, i.e., the relationship between detection probability and false alarm probability) and computational complexity. The radial target velocity v_r was 1.4 m/s, and the CNR was 13 dB. For the conventional PD-STAP, we chose $K = 32$ (i.e., RMB rule [10]) for the CCM estimation. Figure 3 shows the ROC curves after 10^5 Monte Carlo experiments. The clutter was modeled as a compound-Gaussian distribution with texture parameter $v = 12$ [17], and the CPI length N_a was 256. The simulation results indicate that the performance of PD-STAP (known matrix) method is optimal, but the covariance is not known in practice. Deviation of the estimated CCM from the true CCM results in the performance loss of the practical PD-STAP (estimated matrix). Comparatively, the proposed detector had a lower false alarm probability for the same detection probability than the practical PD-STAP (estimated matrix). Figure 4 presents the computational complexity versus the channel numbers with $N_r = 1024$. For the proposed method, curves of different target numbers were drawn. The results show that, with the increase in the number of radar channels n and search N_v, the computational complexity of the PD-STAP sharply increased, while

that of the proposed method slowly increased. Therefore, the proposed method has a simpler computational complexity. In summary, the proposed method provides good performance and potential for real applications since PD-STAP is limited by training data size and content.

Table 1. System parameters.

Quantity	Symbol	Value
Speed of light	c	2.979×10^8 m/s
Center frequency	f_c	10 GHz
Bandwidth	B_r	600 MHz
Number of receive channels	n	4
Pulse repetition frequency	PRF	2000 Hz
Antenna length	L_a	0.38 m
Altitude of the platform	H	3600 m
Central incidence elevation angle	θ_c	63°
Mean slant range	R_c	6.8 km
Platform velocity	v_p	64 m/s
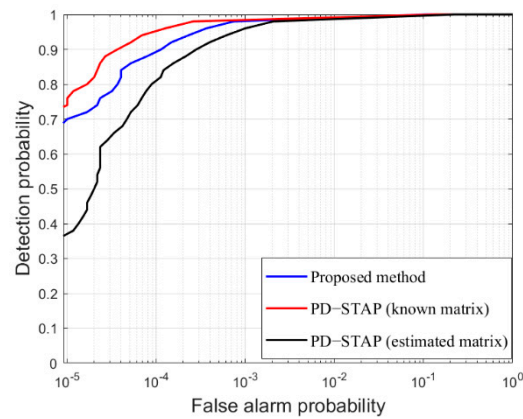
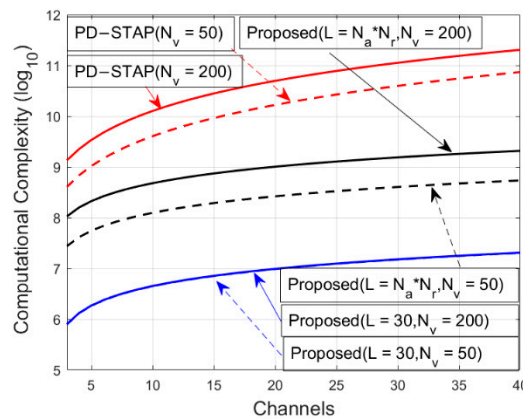**Figure 3.** Receiver operating characteristic (ROC) curves.

Figure 4. Computational complexity versus channel numbers.

4.2. Real Data of Airborne Multichannel Radar

The Aerospace Information Research Institute, Chinese Academy of Sciences (AIR-CAS), conducted experiments using the X/P-SAR system, which is uniformly configured with four independent channels along the track direction. The X/P-SAR sensor was installed on a Cessna 208, as depicted in Figure 5, and the system parameters were as shown in Table 1. For the test site, electric tricycles were used as cooperative moving targets, and they were equipped with radar reflectors to enhance the RCS, as well as with global

positioning system (GPS) to gain geographical reference positions and velocities for GMTI algorithm verification, as shown in Figure 6. The sizes of the two cooperative targets were 1.5 m × 0.88 m × 1.6 m and 1.85 m × 0.9 m × 1.58 m.

Figure 5. X/P-SAR system installed on Cessna 208.

Figure 6. Two cooperative targets.

To demonstrate the effectiveness of the proposed detector, we also provide the results of conventional PD-STAP [12]. $K = 90$ training data were used to estimate the clutter covariance matrix. The range-Doppler image of the first channel is shown in Figure 7, which was generated using 256 azimuth and 3500 range samples. Since the stationary clutter signal was acquired by radar antennas with identical view angle and a time delay on the order of a millisecond, the images were highly correlated. Obviously, there were many strong discrete scatterers in the scene. T1 and T2 were masked by strong clutter due to the slow velocities and low RCSs. Figure 8a,b show the images after clutter suppression. It can be observed that the modified multichannel DPCA had better performance. For the implemented conventional PD-STAP detector, many discrete scatterers were not cancelled, which would be false alarm points. Figure 9 shows the output normalized SCNR of T1. For the proposed method, the SCNR was approximately 28 dB, and the highest background peak was 23 dB below the target. For PD-STAP, the SCNR was approximately 22 dB, and the highest background peak was 17 dB. Furthermore, the SCNR of the exo-clutter region decreased due to the power loss of the target signal. Figure 10 shows the output normalized SCNR of T2. For the proposed method, the SCNR was approximately 30 dB, and the highest background peak was 25 dB below the target. For PD-STAP, the SCNR was approximately 26 dB, and the highest background peak was 21 dB. Thus, the proposed method outperformed PD-STAP by approximately 5 dB.
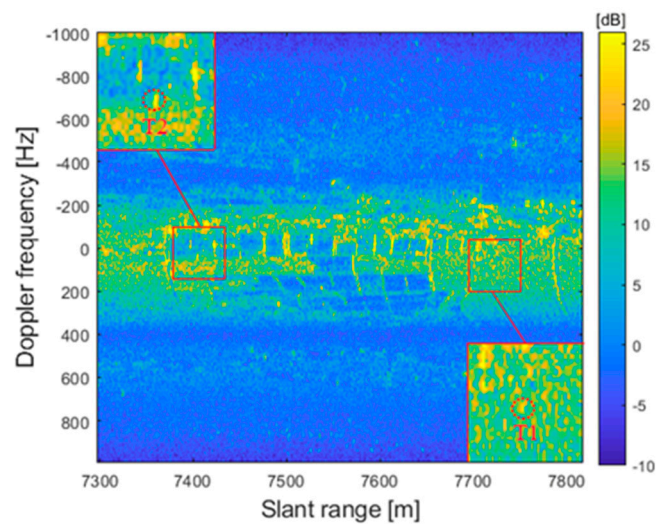
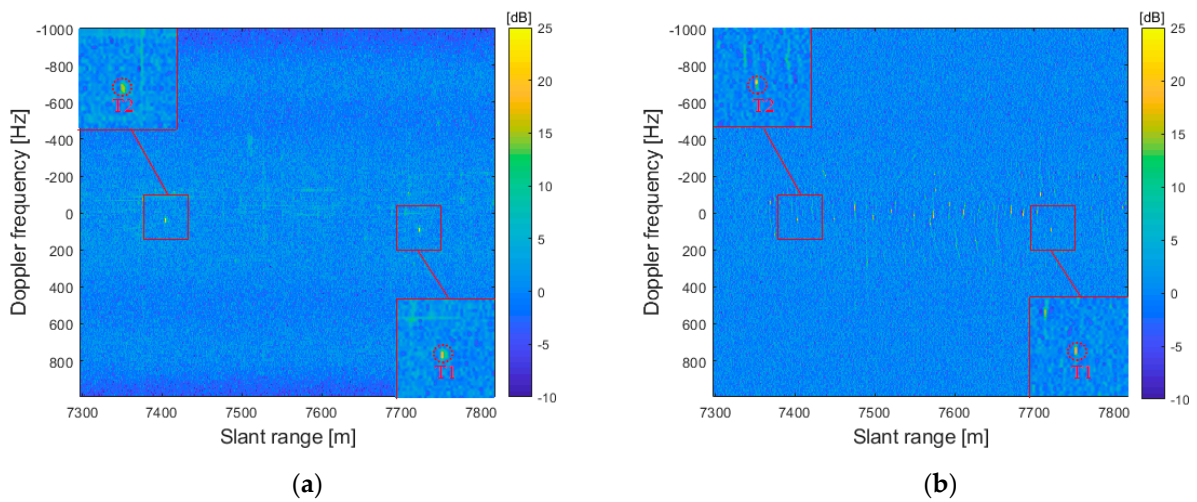**Figure 7.** Range-Doppler image before clutter suppression.

(**a**)   (**b**)

Figure 8. Range-Doppler images: (**a**) the proposed method; (**b**) PD-STAP.

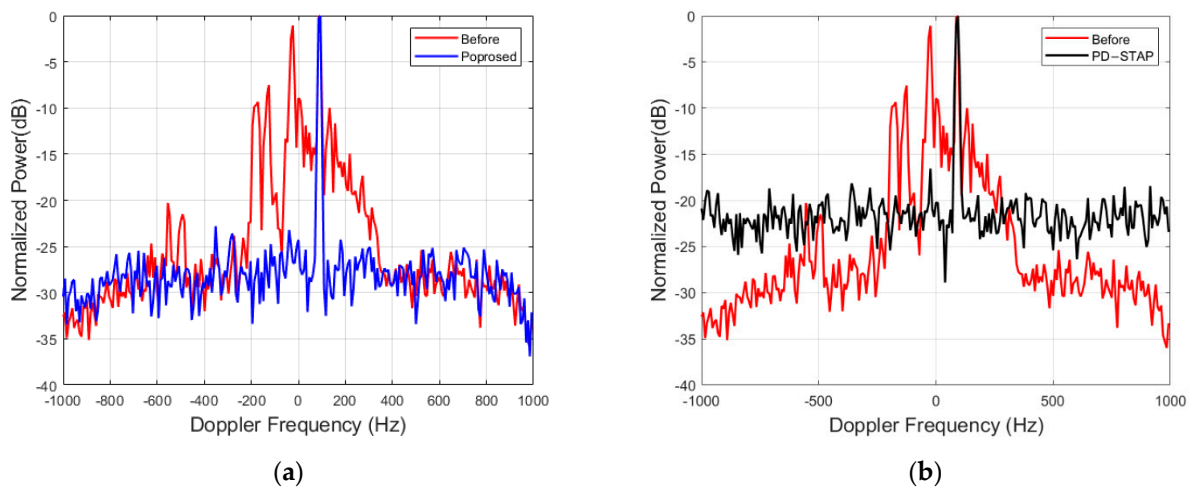(**a**)   (**b**)

Figure 9. Output normalized SCNR of T1: (**a**) the proposed method; (**b**) PD-STAP.
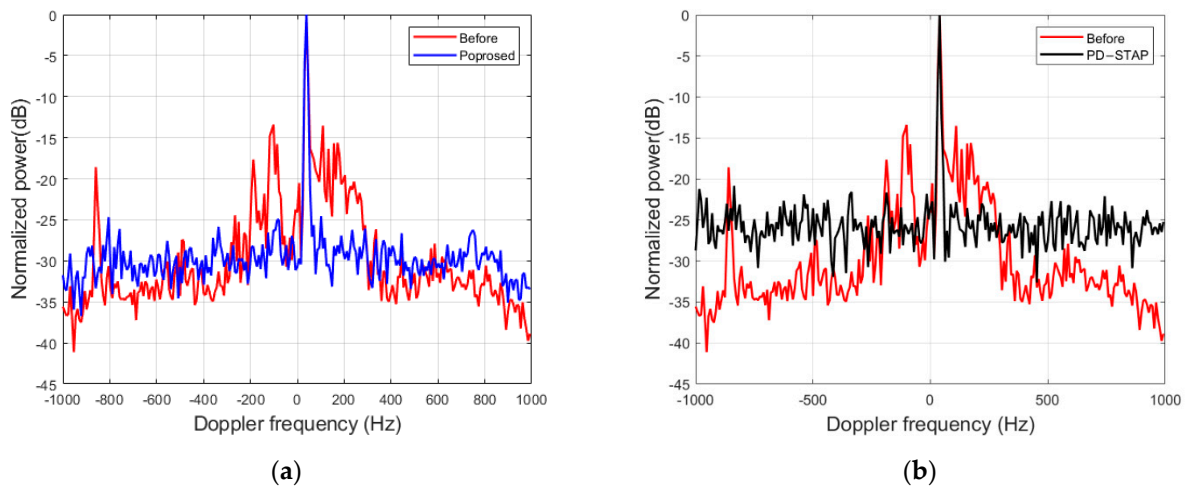
Figure 10. Output normalized SCNR of T2: (**a**) the proposed method; (**b**) PD-STAP.

Figure 11a shows the range-Doppler image with superimposed moving target detections by the amplitude detector. Many false detections are observable. Figure 11b shows the results of the phase detector assisted by the amplitude detector based on the CDP step. Fewer false detections are observable, which shows that the interferometric phase detector with the amplitude detector could significantly reduce the false detections. Multiple CPIs can be utilized to suppress radial scatterers. Figures 12 and 13 show the velocity estimation function P_{out} of T1 and T2, respectively. The radial velocities were estimated from the peak position of the velocity estimation functions, as presented in Table 2. True velocities were recorded by GPS equipment mounted on the motorcycle during the experiment. The velocity estimation errors were estimated as 0.11 m/s and 0.14 m/s for T1 and T2, respectively, which is better than the 0.31 m/s and 0.21 m/s of PD-STAP. Therefore, compared with PD-STAP, the proposed method obtained a very accurate estimation. Moreover, the processing time of the proposed method was approximately reduced by a factor of 34. Thus, in a real-world example, the proposed method outperformed PD-STAP in terms of detection performance and estimation accuracy since the performance of PD-STAP was severely limited by the computational complexity and improper CCM caused by heterogeneous clutter.
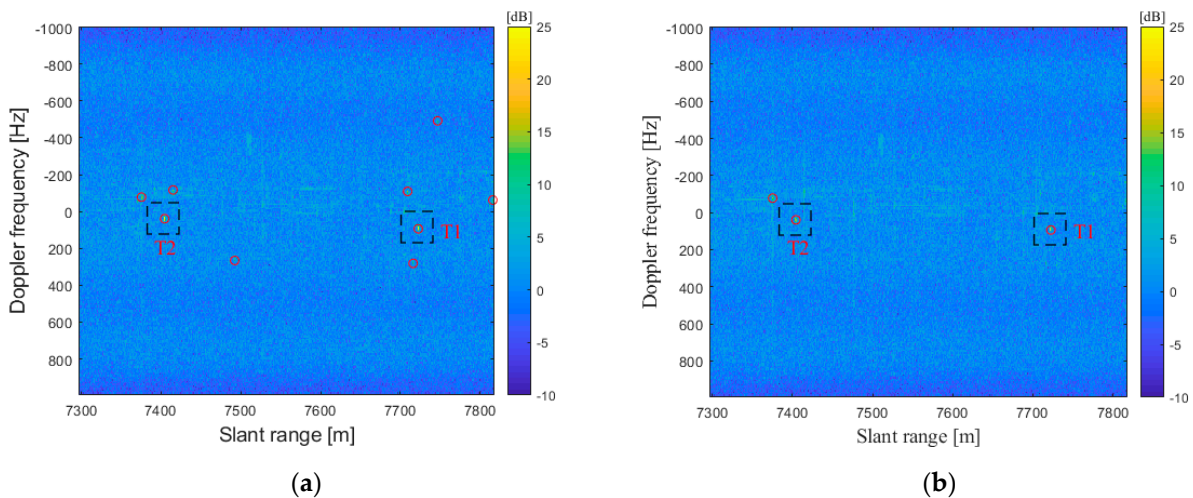

Figure 11. Range-Doppler image of the moving target detection: (**a**) amplitude detector; (**b**) phase detector with amplitude assistance.
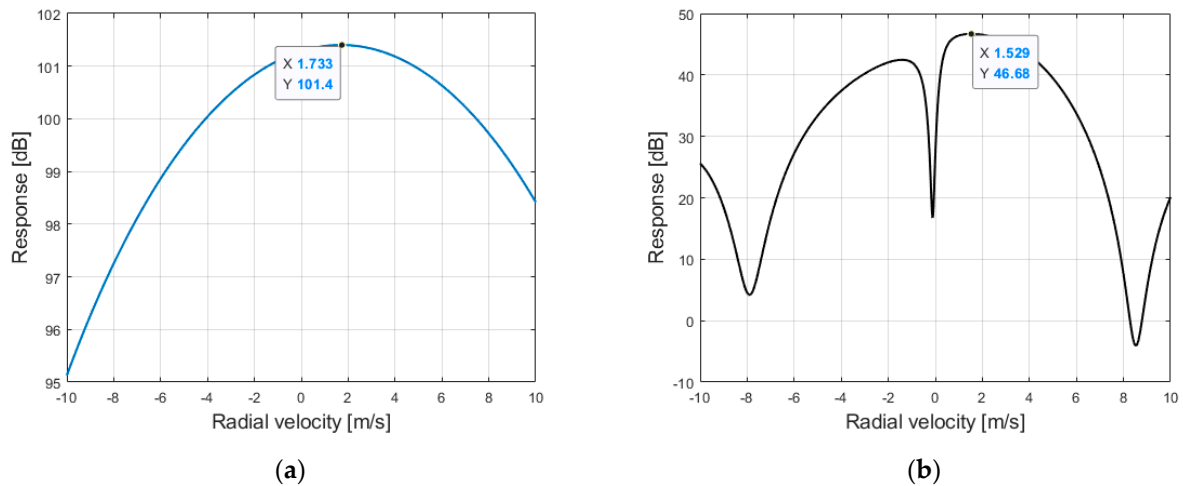
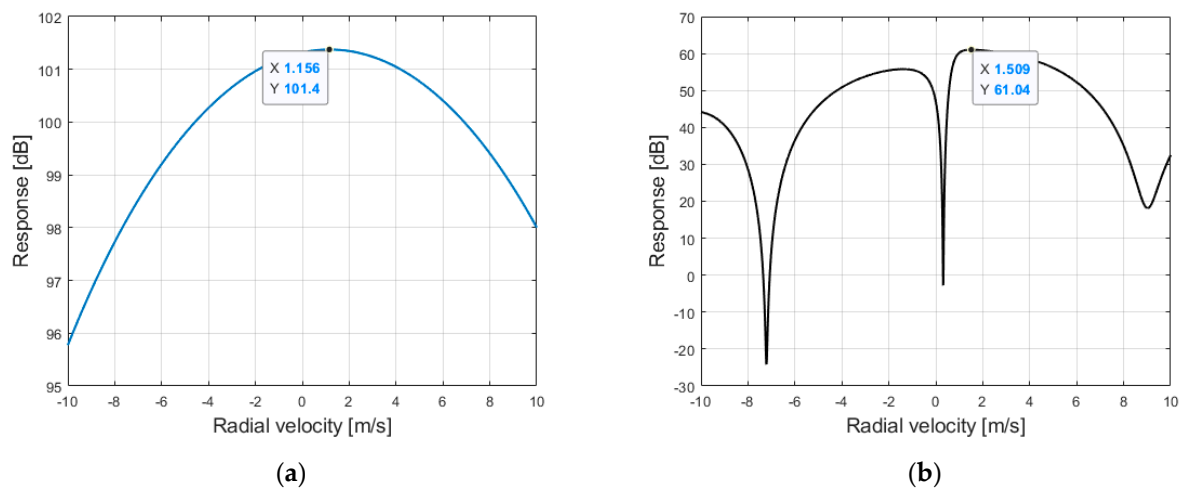**Figure 12.** Velocity estimation function P_{out} of T1: (**a**) the proposed method; (**b**) PD-STAP.

Figure 13. Velocity estimation function P_{out} of T2: (**a**) the proposed method; (**b**) PD-STAP.

Table 2. Target radial velocity estimation.

Target ID	True Velocity	Algorithm	Estimated Velocity	Velocity Error
T1	1.84 m/s	Proposed method	1.73 m/s	0.11 m/s
		PD−STAP	1.53 m/s	0.31 m/s
T2	1.30 m/s	Proposed method	1.16 m/s	0.14 m/s
		PD−STAP	1.51 m/s	0.21 m/s

5. Conclusions

Airborne multichannel radar-GMTI is an important research subject in military and civilian applications. In this paper, the detection and estimation of slow and low-RCS moving targets were studied in the range-Doppler domain, and a novel method was proposed. Specifically, the detection step was performed by combined interferometric phase detection obtained by the CDP with complementary amplitude detection, and the estimation step was achieved by a matched filter bank. The theory of the proposed method and its mathematical framework were also introduced.

Compared with previous detectors, the proposed algorithm has three main characteristics. Firstly, it significantly enhances the detection performance by setting individual

moderate thresholds for the interferometric phase and amplitude. Secondly, its processing efficiency is high, making it suitable for real-time application. The proposed method requires short CPI data, and it does not involve CCM estimation and inversion. Thirdly, it is robust in heterogeneous clutter because it makes no assumptions about the clutter environment.

The developed method was applied to a dataset acquired from the airborne multichannel X/P-SAR system. The data processing results showed that the proposed method offered a sufficiently low probability of false alarms and high processing efficiency. Moreover, the estimation accuracy of radial velocity was on the order of 0.1 m/s. Future investigations will be properly designed to work with a high-performance graphics processing unit as an effective way to achieve onboard real-time GMTI processing.

Author Contributions: Conceptualization, B.W., M.X., and C.S.; investigation, C.S.; software, C.S. and Z.W.; writing—original draft preparation, C.S.; writing—review and editing, C.S., W.X., Y.W., and X.S. All authors have read and agreed to the published version of the manuscript.

Data Availability Statement: Not applicable.

Conflicts of Interest: The authors declare no conflict of interest.

References

1. Budillon, A.; Gierull, C.H.; Pascazio, V.; Schirinzi, G. Along-Track Interferometric SAR Systems for Ground-Moving Target Indication: Achievements, Potentials, and Outlook. *IEEE Geosci. Remote Sens. Mag.* **2020**, *8*, 46–63. [CrossRef]
2. Suwa, K.; Yamamoto, K.; Tsuchida, M.; Nakamura, S.; Wakayama, T.; Hara, T. Image-Based Target Detection and Radial Velocity Estimation Methods for Multichannel SAR-GMTI. *IEEE Trans. Geosci. Remote Sens.* **2017**, *55*, 1325–1338. [CrossRef]
3. Cerutti-Maori, D.; Klare, J.; Brenner, A.R.; Ender, J.H.G. Wide-Area Traffic Monitoring With the SAR/GMTI System PAMIR. *IEEE Trans. Geosci. Remote Sens.* **2008**, *46*, 3019–3030. [CrossRef]
4. Chen, X.; Cheng, Y.; Wu, H.; Wang, H. Heterogeneous Clutter Suppression for Airborne Radar STAP Based on Matrix Manifolds. *Remote Sens.* **2021**, *13*, 3195. [CrossRef]
5. Song, C.; Wang, B.; Xiang, M.; Dong, Q.; Wang, Y.; Wang, Z.; Xu, W.; Wang, R. A General Framework for Slow and Weak Range-Spread Ground Moving Target Indication Using Airborne Multichannel High-Resolution Radar. *IEEE Trans. Geosci. Remote Sens.* **2022**, *60*, 5113616. [CrossRef]
6. Raney, R.K. Synthetic Aperture Imaging Radar and Moving Targets. *IEEE Trans. Aerosp. Electron. Syst.* **1971**, *AES-7*, 499–505. [CrossRef]
7. Lightstone, L.; Faubert, D.; Rempel, G. Multiple Phase Centre DPCA for Airborne Radar. In Proceedings of the 1991 IEEE National Radar Conference, Los Angeles, CA, USA, 12–13 March 1991; pp. 36–40.
8. Liu, B.; Yin, K.; Li, Y.; Shen, F.; Bao, Z. An Improvement in Multichannel SAR-GMTI Detection in Heterogeneous Environments. *IEEE Trans. Geosci. Remote Sens.* **2015**, *53*, 810–827. [CrossRef]
9. Wang, Z.; Wang, Y.L.; Xing, M.; Sun, G.-C.; Shuangxi, Z.; Xiang, J. A Novel Two-Step Scheme Based on joint GO-DPCA and Local STAP in Image Domain for Multichannel SAR-GMTI. *IEEE J. Sel. Top. Appl. Earth Obs. Remote Sens.* **2021**, *14*, 8259–8272. [CrossRef]
10. Ward, J. Space-Time Adaptive Processing for Airborne Radar. In Proceedings of the IEE Colloquium on Space-Time Adaptive Processing, London, UK, 6 April 1998.
11. Robey, F.C.; Fuhrmann, D.R.; Kelly, E.J.; Nitzberg, R. A CFAR Adaptive Matched-Filter Detector. *IEEE Trans. Aerosp. Electron. Syst.* **1992**, *28*, 208–216. [CrossRef]
12. da Silva, A.B.C.; Baumgartner, S.V.; Krieger, G. Training Data Selection and Update Strategies for Airborne Post-Doppler STAP. *IEEE Trans. Geosci. Remote Sens.* **2019**, *57*, 5626–5641. [CrossRef]
13. Yadin, E. Evaluation of noise and clutter induced relocation errors in SAR MTI. In Proceedings of the Proceedings International Radar Conference, Alexandria, VA, USA, 8–11 May 1995; pp. 650–655.
14. Kirk, J.C. Motion Compensation for Synthetic Aperture Radar. *IEEE Trans. Aerosp. Electron. Syst.* **1975**, *AES-11*, 338–348. [CrossRef]

15. Perry, R.P.; DiPietro, R.C.; Fante, R.L. Coherent Integration With Range Migration Using Keystone Formatting. In Proceedings of the 2007 IEEE Radar Conference, Waltham, MA, USA, 17–20 April 2007; pp. 863–868.
16. da Silva, A.B.C.; Baumgartner, S.V.; de Almeida, F.Q.; Krieger, G. In-Flight Multichannel Calibration for Along-Track Interferometric Airborne Radar. *IEEE Trans. Geosci. Remote Sens.* **2020**, *59*, 3104–3121. [CrossRef]
17. Gierull, C.H.; Sikaneta, I.; Cerutti-Maori, D. Two-Step Detector for RADARSAT-2′s Experimental GMTI Mode. *IEEE Trans. Geosci. Remote Sens.* **2013**, *51*, 436–454. [CrossRef]
18. da Silva, A.B.C.; Baumgartner, S.V. Novel post-Doppler STAP with a priori knowledge information for traffic monitoring applications: Basic idea and first results. *Adv. Radio Sci.* **2017**, *15*, 77–82. [CrossRef]
19. Barbarossa, S.; Farina, A. Detection and imaging of moving objects with synthetic aperture radar. Part 2: Joint time-frequency analysis by Wigner-Ville distribution. *IEE Proc. F Radar Signal Process.* **1992**, *139*, 89–97. [CrossRef]
20. Cristallini, D.; Pastina, D.; Colone, F.; Lombardo, P. Efficient Detection and Imaging of Moving Targets in SAR Images Based on Chirp Scaling. *IEEE Trans. Geosci. Remote Sens.* **2013**, *51*, 2403–2416. [CrossRef]
21. Wang, P.; Li, H.; Himed, B. A Parametric Moving Target Detector for Distributed MIMO Radar in Non-Homogeneous Environment. *IEEE Trans. Signal Process.* **2013**, *61*, 2282–2294. [CrossRef]